Received: 24 October 2022 | Revised: 18 April 2023 | Accepted: 13 May 2023

IET Generation, Transmission & Distribution

DOI: 10.1049/gtd2.12874

The Institution of Engineering and Technology WILEY

ORIGINAL RESEARCH

Transient stability versus damping of electromechanical oscillations in power systems with embedded multi-terminal VSC-HVDC systems

Javier Renedo[1] | Luis Rouco[2] | Aurelio Garcia-Cerrada[2] | Lukas Sigrist[2]

[1]ETSI ICAI, Universidad Pontificia Comillas, Madrid, Spain

[2]Instituto de Investigación Tecnológica (IIT), ETSI ICAI, Universidad Pontificia Comillas, Madrid, Spain

Correspondence
Aurelio Garcia-Cerrada, Instituto de Investigación Tecnológica (IIT), ETSI ICAI, Universidad Pontificia Comillas, Madrid, Spain.
Email: aurelio@iit.comillas.edu

Pre-print: J. Renedo, L. Rouco, A. Garcia-Cerrada, L. Sigrist, "Coordinated control in multi-terminal VSC-HVDC systems to improve transient stability: Impact on electromechanical-oscillation damping," arXiv:2208.00083, Online: https://doi.org/10.48550/arXiv.2208.00083 (accessed 12-10-2022), pp. 1-17, 2022.

Funding information
Spanish Government and MCI/AEI/FEDER (EU), Grant/Award Number: RTI2018-098865-B-C31; Madrid Regional Government, Grant/Award Number: P2018/EMT-4366

Abstract

Multi-terminal high-voltage direct current technology based on voltage-source converter stations (VSC-MTDC) is expected to be one of the most important contributors to the future of electric power systems. In fact, among other features, it has already been shown how this technology can contribute to improve transient stability in power systems by the use of supplementary controllers. Along this line, this paper will investigate in detail how these supplementary controllers affect electromechanical oscillations, by means of small-signal stability analysis. The paper analyses two control strategies based on the modulation of active-power injections (P-WAF) and reactive-power injections (Q-WAF) in the VSC stations which were presented in previous work. Both control strategies use global signals of the frequencies of the VSC-MTDC system and they presented significant improvements on transient stability. The paper will provide guidelines for the design of these type of controllers to improve both large- and small-disturbance angle stability. Small-signal stability analysis (in Matlab) has been compared with non-linear time domain simulation (in PSS/E) to confirm the results using CIGRE Nordic32A benchmark test system with a VSC-MTDC system. The paper analyses the impact of the controller gains and communication latency on electromechanical-oscillation damping. The main conclusion of the paper is that transient-stability-tailored supplementary controllers in VSC-MTDC systems can be tuned to damp inter-area oscillations too, maintaining their effectiveness.

1 | INTRODUCTION

Multi-terminal high voltage direct current systems based on voltage source converters (VSC-HVDC) is a key technology for bulk power transmission and for the integration of renewable resources into power systems [1–3]. This enabler technology has received attention worldwide [4] and several conceptual large VSC-HVDC grids have already been proposed in the literature. For example, in Europe, an HVDC-based *supergrid* has been proposed for bulk power transmission through different countries and integration of offshore wind energy [1, 2]. In North America, a *Macrogrid* consisting of several interregional HVDC interconnections has been proposed for massive integration of renewable energy sources [5, 6]. Similarly, an HVDC-based *hypergrid* has been proposed in Italy [7]. Meanwhile, actual examples of multi-terminal VSC-HVDC systems in operation in China are Zhoushan 5-terminal HVDC system [8], Nan'ao 3-terminal HVDC system [9–11] and Zhangbei 4-terminal system [12].

Power-electronic-based devices are expected to have a relevant impact on power system stability [13], for small-disturbance [14–17] and large-disturbance phenomena [18]. Although it is clear that the main aplication of VSC-HVDC systems is power transmission, they can also help to improve the operation of power systems by means of supplementary controllers [19–22]. Previous publications have proposed supplementary controllers in multi-terminal VSC-HVDC systems (VSC-MTDC) to improve rotor-angle stability against small disturbances (electromechanical oscillations, that is,

power-oscillation damping, POD) and against large disturbances (transient stability).

The work in [23] proposed controllers in VSC-HVDC links to damp electromechanical oscillations (also known as power-oscillation-damping (POD) controllers), by modulating active-power (P) through a VSC-HVDC link and reactive-power (Q) injections at both converter stations. The controllers were designed using on robust control techniques. Ref. [24] analysed POD controllers in VSC-HVDC systems, using active-power flow through the link as output signal, and the frequency difference between the two AC terminals of the link as input signal. The paper discussed the design of the gain of the POD controller. The work in [25, 26] proposed POD controllers in VSC-MTDC systems, where the VSCs modulate their P injections using the information from a Wide Area Measurement System (WAMS). The work in [27] proposed POD controllers in DC-voltage-droop-controlled VSC-MTDC systems. In this control strategy, one converter of the VSC-MTDC changes its DC-voltage set point proportionally to the locally measured frequency deviation, using the concept of DC-voltage loop shaping. The work in [28] proposed POD controllers in VSC-MTDC systems to modulate P and reactive-power (Q) injections of the VSCs and using global measurements of the frequencies at the connection points of the VSC stations of the MTDC system. The work in [29] proposed the concept of *virtual friction*, applied to P injections of VSC-MTDC systems interconnecting asynchronous AC areas, to damp electromechanical oscillations and to improve the performance of the overall system. Ref. [30] proposed POD controllers in a VSC-HVDC link embedded in an AC grid based on Linear Matrix Inequality (LMI) optimisation and modulating P/Q injections at the converter stations. POD controllers in VSC-MTDC systems of the references discussed above presented promising results. The work in [31] proposed POD controllers in VSC-MTDC systems embedded in the power system using model predictive control, showing good results. Active-power injections are the input signals and the controllers require information from a WAMS. Ref. [32] showed that POD controllers could also be implemented in offshore wind warms connected through VSC-HVDC links, taking advantage of the energy stored in the capacitors of the DC side.

The improvement of transient stability of a power system using a VSC-MTDC system has already been addressed in the literature. The work in [33] proposed a control strategy in VSC-MTDC systems for transient-stability improvement, where VSC stations control their P injections based on a bang-bang controller and using the speed deviations of the generators with respect to the speed of the centre of inertia (COI) as input signals. Ref. [34] proposed controlling P injections of the VSC stations of a MTDC system based on a sliding-mode strategy and also using global measurements. The work in [35] proposed a control strategy where VSC stations controlled their P injections, using global measurements of the frequencies of the MTDC system. This control strategy is a generalisation of the one proposed in [36] for point-to-point VSC-HVDC links, which modulates the active power transmitted through the link proportionally to the frequency deviation between the two AC terminals of the link. The work in [37] used the same input signal as in [35], but to control the Q injections of the VSC stations. The work in [38] proposed an active-power control strategy in VSC-MTDC systems using global measurements of the angles and frequencies at the connection point of the VSC stations.

In general, small- and large-signal rotor-angle stability are related and improving the latter often improves the former too, and vice-versa. However, this is not a always the case. For example, the study presented in [39] shows that an increase in the gain of the PSS of a synchronous generator improves the damping ratios of electromechanical modes, while transient stability deteriorates, in the system analysed. In the publications discussed above of POD controllers and transient-stability-tailored controllers in VSC-MTDC systems, each work focuses on the particular application of each controller. However, these studies do not focus on the impact of the controllers on both rotor-angle stability phenomena together. Hence, the following questions remain open:

- What is the impact of transient-stability-tailored controllers in VSC-MTDC systems on electromechanical-oscillation damping?
- Could transient-stability-tailored controllers in VSC-MTDC systems help to damp electromechanical oscillations too and play the role of POD controllers?

This paper addresses these two questions and studies the impact of transient-stability-tailored supplementary controllers in VSC-MTDC systems on electromechanical-oscillation damping by means of small-signal stability analysis. The paper analyses two control strategies based on the modulation of active-power injections (P-WAF) [35] and reactive-power injections (Q-WAF) [37] in the VSC stations of the MTDC system. Both control strategies use global signals of the frequencies of the VSC-MTDC system and they presented significant improvements on transient stability. Results suggest guidelines for the design of these type of controllers to improve both, large- and small-disturbance angle stability. Small-signal stability analysis techniques (in Matlab) will be used to assess electromechanical-oscillation damping, while non-linear time domain simulation (in PSS/E) will be used to confirm the results. Contributions will be illustrated in the Nordic32A test system with an embedded VSC-MTDC system. The paper analyses the impact of the controller gains and communication latency on electromechanical-oscillation damping.

Preliminary results were presented by the authors in [40], where a small-signal stability analysis of strategy P-WAF was carried out in a small test system. This paper extends the results an analyses not only the modulation of P injections (P-WAF), but also the modulation of Q injections (Q-WAF) and simultaneous modulation of P and Q injections (PQ-WAF). Furthermore, this paper presents the results in a larger test system (Nordic32A benchmark system) and it analyses the impact of communication latencies on the performance of the control strategies, which was not analysed in [40].

The rest of the paper is organised as follows. Section 2 describes how VSC-MTDC systems are modelled. Section 3

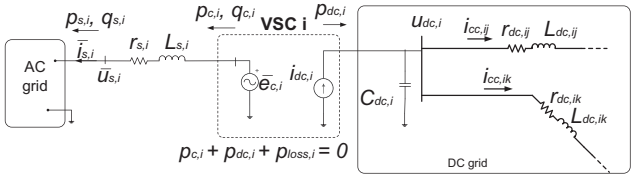

FIGURE 1 VSC and the HVDC grid based on the principles of [41].

describes the transient-stability-tailored control strategies in VSC-MTDC systems which will be analised in the paper. Section 4 presents the results obtained in the paper. Section 5 presents the conclusions obtained in this work. Finally, the Appendix contains the data used.

2 | MODELLING OF MULTI-TERMINAL VSC-HVDC SYSTEMS

In VSC-MTDC systems, more than two VSC stations are connected to the same HVDC grid. Figure 1 depicts the dynamic model of a VSC connected to an HVAC grid and to an HVDC grid, following the guidelines of [41–44] for electromechanical-type models of these types of systems (type-6 models, according to the classification of reference [45]). Outer control loops of VSCs are modelled in detail, while inner current control loops are approximated by a first-order transfer function between the current references and their actual values.

All the details of the dynamic model for VSC-MTDC systems used in this work can be found in [46] and, therefore, they are not included in this paper. The details of the linearised model used for small-signal stability analysis can be found in [40]. The initial operating point of the VSC-MTDC system is obtained with the AC/DC power flow method proposed in [47].

3 | CONTROL STRATEGIES

The control strategies to be investigated were proposed and described in detail in in [35, 37] and this paper will analyse their impact on electromechanical-oscillation damping. Only the key aspects of the controllers are described in this section, in order to make the paper self contained.

When a disturbance occurs in a power system, bus frequencies change and, during the transient, frequencies at different buses of the system are not the same [48, 49]. This is the main reason why control strategies for transient stability improvement using global measurements (such as generator speeds or the speed of the COI) have proved to be effective in different contexts [33, 50].

In the control strategies to be analysed in this work, global-but-practical measurements are used: they use global information of the dynamic behaviour of the system, but restricting the communication system between the converter stations of the VSC-MTDC system. Every converter of the VSC-MTDC system compares its own frequency measured at the AC bus with a frequency set point, which is calculated as the

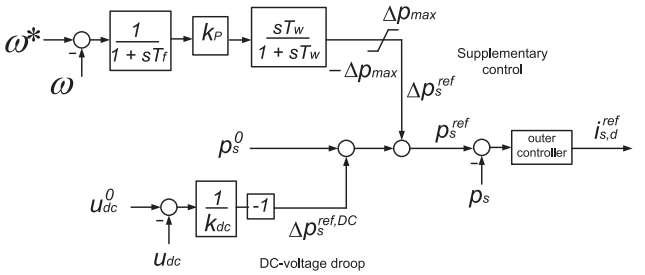

FIGURE 2 Strategy P-WAF. Frequency in pu.

weighted average of the frequencies measured at the AC side of the VSC stations (weighted-averaged frequency, WAF):

$$\omega^* = \bar{\omega} = \sum_{k=1}^{n} \alpha_k \omega_k \text{ (pu)}, \alpha_k \in [0, 1], \sum_{k=1}^{n} \alpha_k = 1. \quad (1)$$

where ω_k is the frequency measured at the AC bus of VSC$_k$ in pu.

The frequency error signal is used by every VSC to modulate its P Injection (strategy P-WAF) and/or its Q injection (strategy Q-WAF).

3.1 | Strategy P-WAF

Figure 2 shows the block diagram of control strategy P-WAF [35], where the frequency set point of the controller is calculated as in (1), which requires a communication system among the converter stations of the VSC-MTDC system, which is a strong but realistic restriction.

The behaviour of strategy P-WAF is as follows. During the transient produced by a disturbance, the frequencies seen the VSCs will change. If a VSC has the frequency above (below) the WAF, it will decrease (increase) its P injection, aiming to pull together the speeds of the generators of the system.

In order to share the control effort among all converters and avoid DC-voltage fluctuations, reference [35] proposed the following relationship between the gains and the weighting coefficients of the WAF:

$$\frac{k_{P,k}}{k_{P,T}} = \alpha_k, \text{ with } k_{P,T} = \sum_{j=1}^{n} k_{P,j}. \quad (2)$$

while making α_k proportional to the nominal apparent power of each VSC$_k$ of the MTDC system.

3.2 | Strategy Q-WAF

Figure 3 shows the block diagram of control strategy Q-WAF [37], where the frequency set point of the controller is also calculated as in (1). The controller is activated only if the AC voltage at the connection point is above a certain threshold V_{TH} ($\gamma = 1$ if $u_s \geq V_{TH}$), to guarantee the control actions only

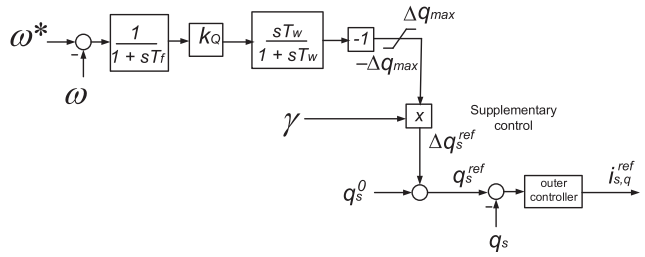

FIGURE 3 Strategy Q-WAF. Frequency in pu.

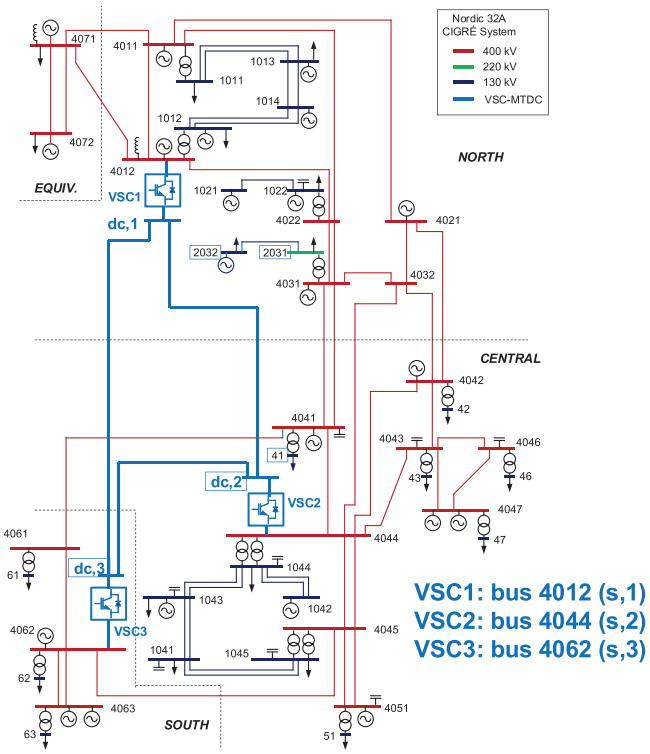

FIGURE 4 Nordic32A system with a VSC-MTDC system.

after the fault is cleared (preventing the controller acting during a short circuit). This precaution improves the performance of the controller.

The behaviour of strategy Q-WAF is as follows. If a VSC has the frequency above (below) the WAF, it will increase (decrease) its Q injection, aiming to pull together the speeds of the generators of the system.

The work in [37] used the following design:

$$\frac{k_{Q,k}}{k_{Q,T}} = \alpha_k,\ k_{Q,T} = \sum_{j=1}^{n} k_{Q,j}. \tag{3}$$

4 | RESULTS

The case study considered consists of the CIGRE Nordic32A benchmark test system [51] with a 3-terminal VSC-HVDC system, as shown in Figure 4. Each VSC has a nominal apparent power of 1000 MVA. A critical scenario with poorly damped inter-area oscillations is considered. The modifications made to stress the system and the data of the VSC-MTDC system are provided in the Appendix.

TABLE 1 Initial operating point of the VSC-MTDC system.

Converter	$P^0_{s,i}$ (MW)	$Q^0_{s,i}$ (MVAr)	$u^0_{s,i}$ (pu)	$u^0_{dc,i}$ (pu)
VSC1	−350.00	0.00	1.0100	1.0006
VSC2	500.00	150.00	0.9982	0.9978
VSC3	−190.08	100.00	1.0149	1.0000

Each VSC of the MTDC system is controlled with DC-voltage droop control and constant reactive power injection. Table 1 depicts the initial steady-state operating point of the VSC-MTDC system, calculated with an AC/DC power flow [46, 47].

The dynamic model of the system in Figure 4 has been linearised around the steady-state operation point and the linearised model has been implemented in Matlab-based Small Signal Stability Tool (SSST) [52], as described in [40]. The linearised system reads:

$$\Delta\dot{\boldsymbol{x}} = \boldsymbol{A}\Delta\boldsymbol{x}. \tag{4}$$

where $\boldsymbol{A} \in \mathbb{R}^{n_x \times n_x}$ is the state matrix, $\Delta\boldsymbol{x} \in \mathbb{R}^{n_x \times 1}$ is the vector of increments of the state variables and n_x is the number of state variables of the system.

Electromechanical oscillations have been identified using eigenvalue techniques and participation-factors [53–55]. The system has two inter-area modes with low damping ratios, as depicted in Table 2.

The information about the electromechanical oscillations between different synchronous machines in the system can be extracted from the right eigenvectors of the linearised system (4), which are known as mode shapes [56]. The right eigenvector $\boldsymbol{v_k} \in \mathbb{C}^{n_x \times 1}$ associated to eigenvalue λ_k satisfies:

$$\lambda_k \boldsymbol{v}_\mathbf{k} = \boldsymbol{A}\boldsymbol{v}_\mathbf{k}. \tag{5}$$

The information of the oscillation of mode λ_k of a certain state variable of (4), x_i, can be analysed with the position of the right eigenvalue associated to the state variable $v_{ik} \in \mathbb{C}$. In particular, the phases of the mode shapes v_{ik} provide information about which state variables oscillate together with or against to other state variables, when a certain mode is excited.

Figures 5 and 6 show the shapes of inter-area modes A and B (right eigenvectors associated to the speeds of the synchronous machines), respectively. In inter-area mode A, synchronous machines in the North oscillate against synchronous machines in the South and in the Centre: mode shapes of the speeds of the generators in the North have opposite phases to mode shapes of the speeds of the generators in the South. In inter-area mode B, synchronous machines in the North and South oscillate against machines in the Centre: mode shapes of the speeds of the generators in the North and South are in phase, while they have

TABLE 2 Inter-area modes.

Mode	Eigenvalue (rad/s)	ζ (%)	Freq. (Hz)	Dominant machines	Oscillation
A	$-0.1044 \pm j3.2333$	3.23	0.51	G4072, G4063	North against South & Centre
B	$-0.3186 \pm j5.2160$	6.10	0.83	G4063, G4072, G1042	North and South against Centre

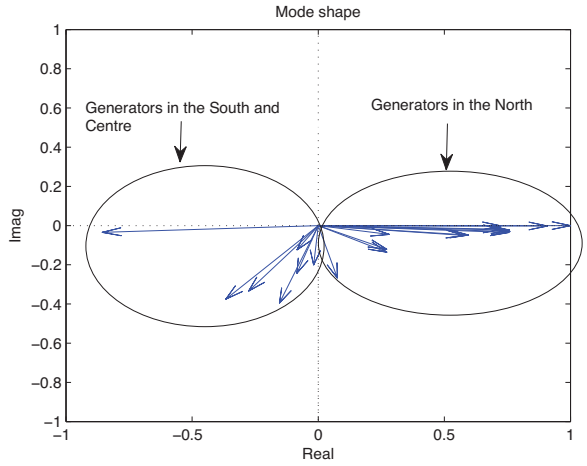

FIGURE 5 Shapes of inter-area mode A.

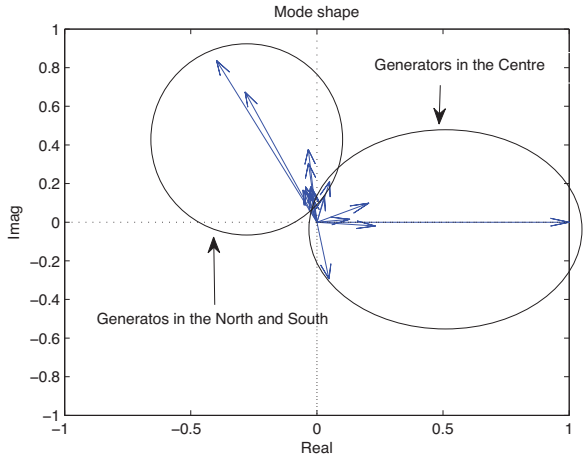

FIGURE 6 Shapes of inter-area mode B.

opposite phases to mode shapes of the speeds of the generators in the South.

4.1 | Small-signal stability analysis

The impact of the controller gains of strategies P-WAF (P injections) and Q-WAF (Qinjections) on inter-area modes is analysed. Gains at all VSC stations were changed (satisfying (2) and (3)) and eigenvalues and their damping ratio were obtained. Since gains in the range $k_{P,i}, k_{Q,i} = [100, 300]$ pu

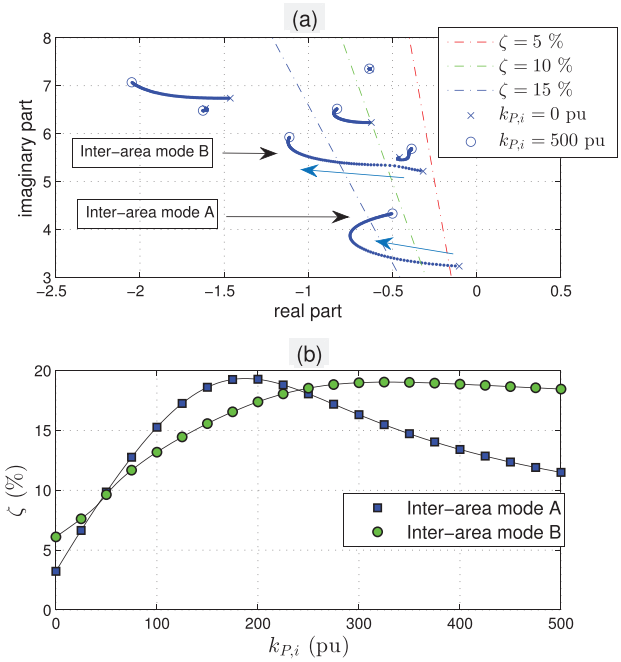

FIGURE 7 Strategy P-WAF. Impact of gains $k_{P,i}$ on (a) evolution of electromechanical modes and (b) damping ratio.

(pu's are referred to the converter rating) proved to be effective to improve transient stability [35, 37]. Now gains $k_{P,i}, k_{Q,i} = [0, 500]$ pu will be explored. The rest of parameters of the control strategies are provided in the Appendix.

Figure 7 shows the evolution of the inter-area modes of the system and their damping ratios as the gains of control strategy P-WAF (P injections) increase. Initially, inter-area mode A moves towards the left-hand side of the complex plane as $k_{P,i}$ increases. However, for high values of the controller gains this trend changes. The damping ratio of inter-area mode A increases as $k_{P,i}$ increases, it reaches its maximum value with $k_{P,i}$ around 200 pu. Inter-area mode B follows a similar pattern. The damping ratio of inter-area mode B increases as $k_{P,i}$ increases and it approximately saturates with $k_{P,i}$ around 300 pu. The damping ratios of inter-area modes A and B are much higher than the ones obtained in the base case, for all values of the controller gain $k_{P,i}$. In addition, notice that controller gains $k_{P,i}$ have small impact on the damping ratio of other modes.

Figure 8 shows the evolution of the inter-area modes of the system and their damping ratios as the gains of control strategy Q-WAF (Q injections) increase. Inter-area mode A moves towards the left-hand side of the complex plane as $k_{Q,i}$ increases

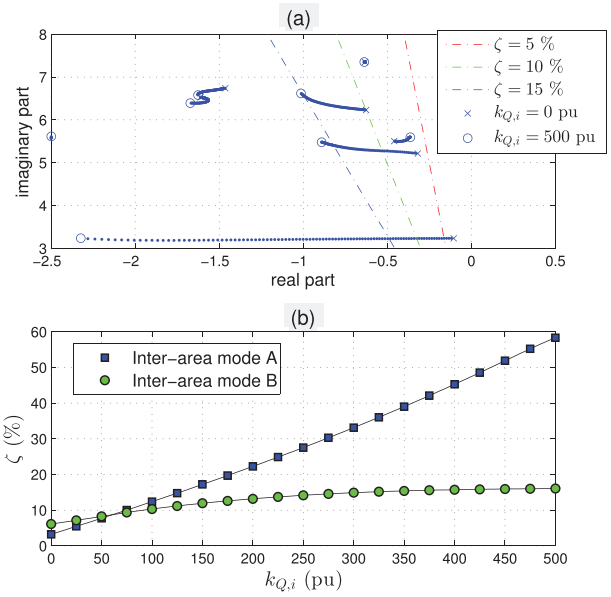

FIGURE 8 Strategy Q-WAF. Impact of gains $k_{Q,i}$ on (a) evolution of electromechanical modes and (b) damping ratio.

and its damping ratio increases, significantly. Inter-area mode B also moves towards the left-hand side of the complex plane as $k_{Q,i}$ increases and its damping ratio also increases. However, the damping ratio of mode B is lower than the one of mode A and saturates. Therefore, controller gains $k_{Q,i}$ have small impact on the damping ratio of other modes.d.

Results prove that with reasonable values of the controller gains for transient-stability improvement in strategies P-WAF and Q-WAF (e.g. $k_{P,i} = k_{Q,i} = 200$ pu), inter-area modes are also damped successfully without affecting other modes significantly. Furthermore, small-signal stability techniques can be used to design the controller gains in order to obtain the required damping ratios of the electromechanical modes.

Notice that the improvements on the damping ratios of inter-area modes achieved with transient-stability-tailored control strategies P-WAF and Q-WAF are comparable to those obtained with specific POD controllers in VSC-HVDC systems (see [23] and [24], for example). The objective of analysing the capability of transient-stability-tailored controllers to damp electromechanical oscillations is not to replace POD controllers and the use of each type of controller would depend on the particular stability phenomenon that is needed to be improved for a certain power system. The objective of this work is to show that the controllers analysed here are an option to improve both phenomena at the same time (rotor-angle stability against large and small disturbances).

4.2 | Non-linear time-domain simulation

The performance of the control strategies has been tested by means of non-linear time domain simulation in PSS/E tool (electromechanical simulation), using the model proposed in [46]. Four cases are compared:

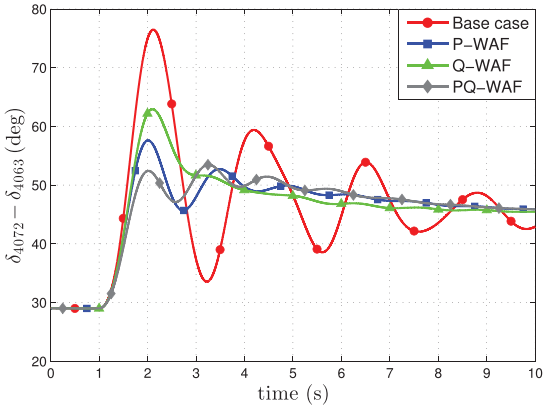

FIGURE 9 Difference of generator angles.

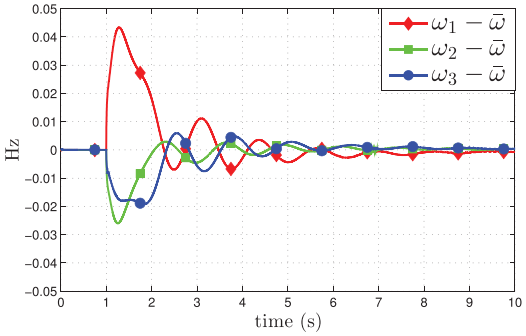

FIGURE 10 Frequency deviations with respect to the weighted-average frequency (case P-WAF).

- Base case: no supplementary control strategy.
- P-WAF: Strategy P-WAF (P injections) (Figure 2), with $k_{P,i} = 200$ pu.
- Q-WAF: Strategy Q-WAF (Q injections) (Figure 3), with $k_{Q,i} = 200$ pu.
- PQ-WAF: Simultaneous modulation of P and Q injections with strategies P-WAF and Q-WAF, with $k_{P,i} = k_{Q,i} = 200$ pu.

The rest of parameters of the control strategies are provided in the Appendix.

Line 4012-4022 (see Figure 4) is tripped at $t = 1$ s. Figure 9 shows the difference between the bus-voltage angles of generators 4072 (North) and 4063 (South). The three control strategies (P-WAF, Q-WAF and PQ-WAF) succeed in damping the inter-area oscillations present in the base case.

Figures 11 and 12 show the active- and reactive-power injections of the VSC stations, respectively. In strategy P-WAF, only P injections are modulated. After the event, the P injection of VSC 1 decreases (P absorption of VSC 1 increases) because its frequency is above the WAF, while the P injections of VSCs 2 and 3 increase because their frequencies are below the WAF (see Figure 10, as an example). Analogously, in strategy Q-WAF, only Q injections are modulated. The behaviour of Q injections in Q-WAF is similar to the behaviour of P injections in P-WAF, but with opposite direction, due to the negative sign of Figure 3.

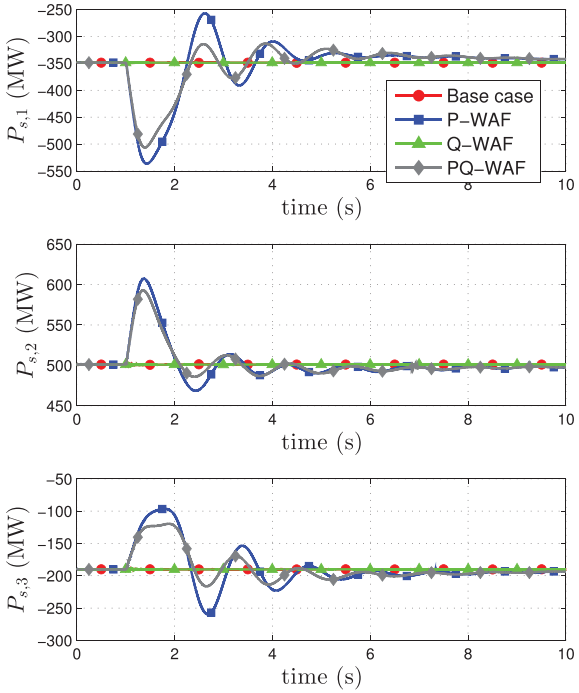

FIGURE 11 Active-power injection of each VSC ($P_{s,i}$).

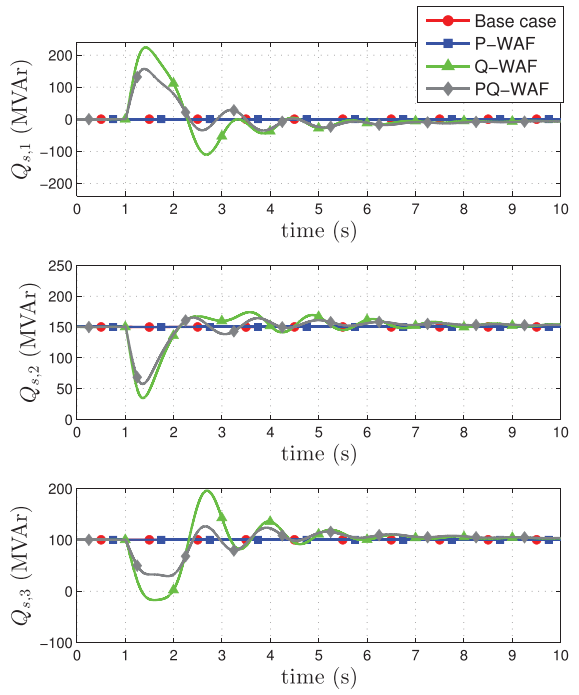

FIGURE 12 Reactive-power injection of each VSC ($Q_{s,i}$).

In strategy PQ-WAF, both, P and Q injections are modulated. Both, modulation of P and/or Q injections of the VSC stations contribute positively to damp inter-area oscillations.

Finally, an extremely severe fault is simulated, in order to compare the performance of the control strategies in terms of transient stability. A three-phase-to-ground short circuit applied to line 4031-4041a (close to bus 4041) (see Figure 4), which is cleared by disconnecting the two circuits of the corridor 100 ms later. Figure 13 shows the difference of generator angles. Synchronism is lost in the base case, while the system is stable with control strategies P-WAF, Q-WAF and PQ-WAF. Hence, the control strategies improve transient stability.

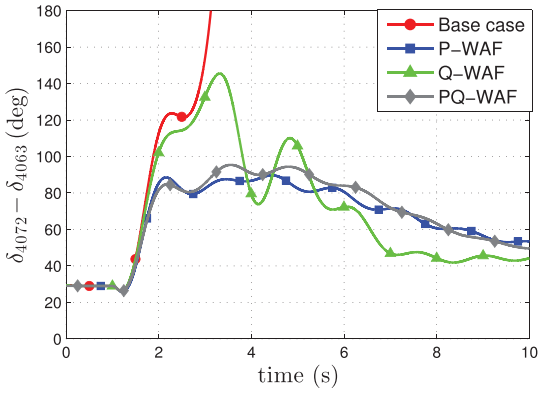

FIGURE 13 Difference of generator angles.

4.3 | Impact of communication latency

The impact of communication latency on the performance of the control strategies is also analysed by introducing a delay in the frequency set point calculated by each VSC (τ) when calculating the WAF in (1):

$$\omega^* = \bar{\omega} e^{-\tau s} \tag{6}$$

A second-order Padé's approximation has been used to represent the transfer function of the delay in (6), as proposed in [57]. Realistic values for the delays ($\tau = 50$ ms and $\tau = 100$ ms) will be tested [58].

The parameters of the control strategies are the same as the ones used in Section 4.2.

4.3.1 | Small-signal stability analysis

Figure 14 shows the evolution of the inter-area modes of the system and their damping ratios as the communication delays, τ, increase when using control strategy P-WAF. Communication latencies has very little effect on the damping ratios of inter-area modes when using strategy P-WAF. This is consistent with the analysis presented in [59]: the DC-voltage droop attenuates significantly the effect of communication latency in strategy P-WAF.

Figure 15 shows the evolution of the inter-area modes of the system and their damping ratios as the communication delays, τ, increase when using control strategy Q-WAF. The damping ratio of inter-area modes decrease as communication delays τ increase, when using strategy Q-WAF. The impact is higher on inter-area mode A. The damping ratios obtained in the presence of communication delays are still much higher than those obtained in the base case.

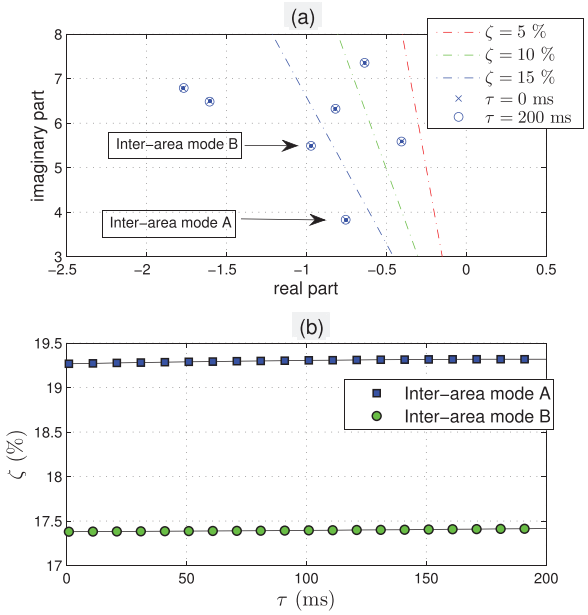

FIGURE 14 Strategy P-WAF. Impact of delay τ on (a) evolution of electromechanical modes and (b) damping ratio.

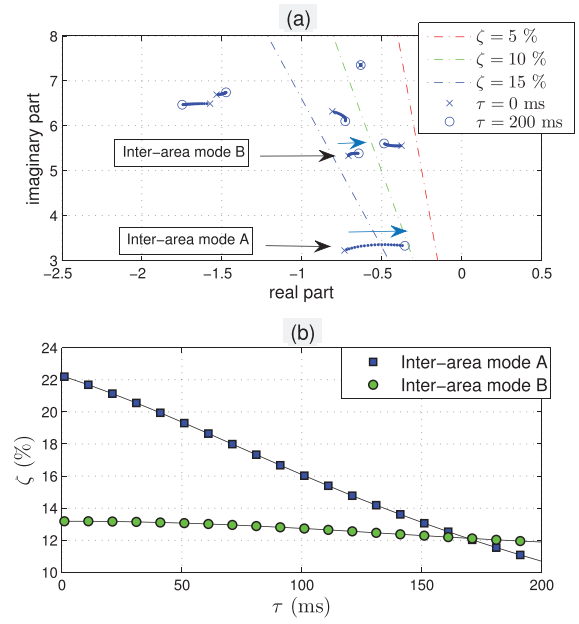

FIGURE 15 Strategy Q-WAF. Impact of delay τ on (a) evolution of electromechanical modes and (b) damping ratio.

4.3.2 | Non-linear time-domain simulation

Communication delays of $\tau = 50$ ms and $\tau = 100$ ms were tested, when using strategies P-WAF, Q-WAF and PQ-WAF. The same disturbance than in previous section has been simulated. Line 4012-4022 is tripped at $t = 1$ s. Figure 16 shows the difference between the bus-voltage angles of generators 4072 and 4063. The three control strategies (P-WAF, Q-WAF and PQ-WAF) succeed in damping the inter-area oscillations

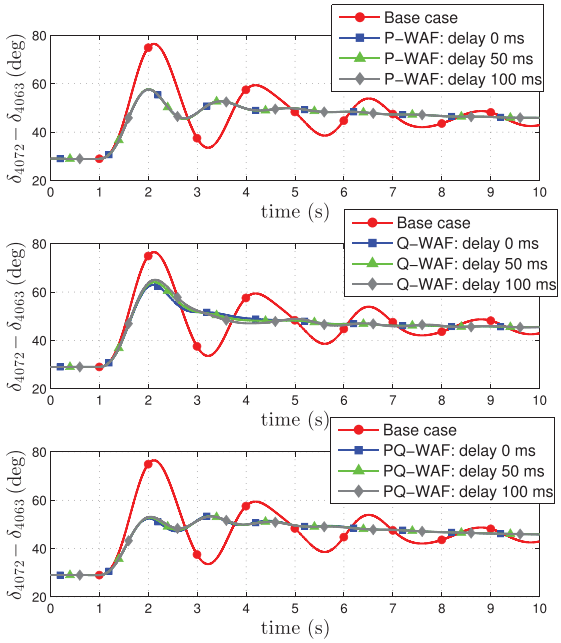

FIGURE 16 Difference of generator angles. Impact of communication delay τ.

present in the base case and the results are very similar to those obtained with no communication latencies.

4.4 | Overall performance

This section analyses the overall performance of the control strategies regarding:

- Rotor-angle stability against large disturbances (transient stability) and
- Rotor-angle stability against small disturbances (electromechanical oscillations)

Transient stability is the main application of control strategies P-WAF, Q-WAF and PQ-WAF and it has been analysed in detail in [35, 37]. Nevertheless, results on transient stability are also included in this paper, for reference, to evaluate the overall performance of the control strategies. Transient-stability margins are quantified using the critical clearing time (CCT), which is defined as the maximum time duration that a fault can stay before clearance without eventually provoking loss of synchronism. An extremely severe fault is selected: a three-phase-to-ground short circuit applied to line 4031-4041a (close to bus 4041) (see Figure 4), which is cleared by disconnecting the two circuits of the corridor (Fault I, for short). At the initial operating point, each circuit of the corridor carries 644.50 MW.

Table 3 shows damping ratios and frequencies of the inter-area modes A and B, and the CCT of Fault I, obtained in the base case and for control strategies P-WAF, Q-WAF and PQ-WAF. In all cases, controller gains are set to $k_{P,i} = k_{Q,i} = 200$ pu and the rest of the parameters as described in the Appendix. The control strategies significantly increase the

TABLE 3 Comparison. EO: Electromechanical oscillations (small disturbance), TS: Transient stability (large disturbance).

Case	EO Mode A ζ (%), f (Hz)	EO Mode B ζ (%), f (Hz)	TS Fault I CCT (ms)
Base case	3.23 %, 0.51 Hz	6.10 %, 0.83 Hz	70 ms
P-WAF, $\tau = 0$ ms	19.27 %, 0.62 Hz	17.38 %, 0.89 Hz	270 ms
P-WAF, $\tau = 50$ ms	19.29 %, 0.62 Hz	17.39 %, 0.89 Hz	270 ms
P-WAF, $\tau = 100$ ms	19.30 %, 0.62 Hz	17.39 %, 0.89 Hz	270 ms
Q-WAF, $\tau = 0$ ms	22.24 %, 0.53 Hz	13.18 %, 0.86 Hz	230 ms
Q-WAF, $\tau = 50$ ms	19.37 %, 0.54 Hz	13.06 %, 0.86 Hz	180 ms
Q-WAF, $\tau = 100$ ms	16.09 %, 0.54 Hz	12.73 %, 0.86 Hz	120 ms
PQ-WAF, $\tau = 0$ ms	22.74 %, 0.71 Hz	21.23 %, 0.91 Hz	320 ms
PQ-WAF, $\tau = 50$ ms	19.21 %, 0.70 Hz	21.06 %, 0.91 Hz	300 ms
PQ-WAF, $\tau = 100$ ms	16.75 %, 0.69 Hz	21.06 %, 0.90 Hz	280 ms

damping ratios of inter-area modes A and B, in comparison with the base case. The damping ratios deteriorate slightly in the presence of communication latency; however the improvements are still significant. The control strategies increase the CCT of Fault I significantly. Communication latencies do not reduce the CCT in strategy P-WAF. This is consistent with the results presented in [59]: the DC-voltage droop attenuates the effect of communication latency when modulating P injections. However, the impact of communication latency is stronger when modulating Q injections with strategy Q-WAF. Nevertheless, results obtained in the presence of communication latency are better than those obtained in the base case.

Hence, results prove that control strategies P-WAF, Q-WAF and PQ-WAF improve both transient stability and electromechanical-oscillation damping, significantly.

5 | CONCLUSIONS

This paper analysed the impact of transient-stability-tailored supplementary controllers in VSC-MTDC systems on electromechanical-oscillation damping, by means of small-signal stability analysis. In the control strategies analysed, each VSC of the MTDC system compares its own frequency with the weighted-average frequency (WAF) of the VSC stations and it modulates its P injection, Q injection or both simultaneously (P-WAF, Q-WAF and PQ-WAF, respectively).

The conclusions obtained in this paper can be summarised as follows:

- Control strategies P-WAF, Q-WAF and PQ-WAF can be tuned to (a) improve transient stability and to (b) damp inter-area electromechanical oscillations too.
- The control strategies produce good results in the presence of communication delays, under small disturbances and under large disturbances.
- Although bulk power transmission and the recollection of non-dispatchable energy sources are the main purposes of a multi-terminal VSC-HVDC system embedded in a conventional HVAC system, the flexibility of VSC stations makes it possible the contribution of these systems to the overall improvement of the power system stability. This contribution adds a remarkable value to this technology and should be taken into account when carrying out a cost-benefit analysis in future developments. The economical benefit of angle-stability controllers is strongly related to the increase of transmission capacity between different areas in large power systems.

AUTHOR CONTRIBUTIONS

Javier Renedo: Conceptualization, formal analysis, investigation, methodology, validation, writing - original draft. Luis Rouco: Conceptualization, investigation, methodology, supervision, validation, writing - review and editing. Aurelio Garcia-Cerrada: Conceptualization, funding acquisition, investigation, methodology, supervision, validation, writing - review and editing. Lukas Sigrist: Conceptualization, investigation, methodology, supervision, validation, writing - review and editing.

ACKNOWLEDGEMENTS

This work was supported by the Gobierno de España and MCI/AEI/FEDER (EU) under Project Ref. RTI2018-098865-B-C31 and by Madrid Regional Government under PROMINT-CM Project Ref. P2018/EMT-4366.

CONFLICT OF INTEREST STATEMENT

The authors have declared no conflict of interest.

DATA AVAILABILITY STATEMENT

The data that support the findings of this study are available from the corresponding author upon reasonable request.

ORCID

Javier Renedo https://orcid.org/0000-0002-1740-8729
Luis Rouco https://orcid.org/0000-0002-2670-7464
Aurelio Garcia-Cerrada https://orcid.org/0000-0003-1950-2927
Lukas Sigrist https://orcid.org/0000-0003-2177-2029

REFERENCES

1. Van Hertem, D., Ghandhari, M.: Multi-terminal VSC HVDC for the European supergrid: Obstacles. Renewable Sustainable Energy Rev. 14(9), 3156–3163 (2010)
2. Bompard, E., Fulli, G., Ardelean, M., Masera, M.: It's a bird, it's a plane, it's a… supergrid. IEEE Power Energy Mag. 12(2), 41–50 (2014)
3. Gomis-Bellmunt, O., Sánchez-Sánchez, E., Arévalo-Soler, J., Prieto-Araujo, E.: Principles of operation of grids of DC and AC subgrids interconnected by power converters. IEEE Trans. Power Delivery 36(2), 1107–1117 (2021)
4. Buigues, G., Valverde, V., Etxegarai, A., Eguía, P., Torres, E.: Present and future multiterminal HVDC systems: Current status and forthcoming developments. In: Proceedings of International Conference on Renewable Energies and Power Quality (ICREPQ), pp. 83–88. IEEE, Piscataway (2017)
5. Figueroa Acevedo, A.L., Jahanbani-Ardakani, A., Nosair, H., Venkatraman, A., McCalley, J.D., Bloom, A., Osborn, D., Caspary, J., Okullo, J., Bakke, J, Scribner, H.: Design and valuation of high-capacity HVDC macrogrid transmission for the continental US. IEEE Trans. Power Syst. 36(4), 2750–2760 (2020)

6. McCalley, J., Zhang, Q.: Macro grids in the mainstream: An international survey of plans and progress. Tech. Rep., Americans for a Clean Energy Grid (ACEG), Macro Grid Initiative (2020)
7. del Pizzo, F., Carlini, E.M., Baffa Scirocco, T., Capurso, P., Dicuonzo, F., Armillei, C., Zanghi, A., Urbanelli, A.: Towards the Italian electricity grid of the future. In: Proceedings of CIGRE Session, pp. 1–10. IET, Stevenage (2022)
8. Pipelzadeh, Y., Chaudhuri, B., Green, T.C., Wu, Y., Pang, H., Cao, J.: Modelling and dynamic operation of the Zhoushan DC grid: Worlds first five-terminal VSC-HVDC project. In: Proceedings of International High Voltage Direct Current 2015 Conference, pp. 87–95 (2015)
9. Li, X., Yuan, Z., Fu, J., Wang, Y., Liu, T., Zhu, Z.: Nanao multi-terminal VSC-HVDC project for integrating large-scale wind generation. In: Proceedings of IEEE/PES General Meeting, National Harbor, pp. 1–5. IEEE, Piscataway (2014)
10. Bathurst, G., Bordignan, P.: Delivery of the Nan'ao multi-terminal VSC-HVDC system. In: Proc. 11th IET International Conference on AC and DC Power Transmission (ACDC), Birmingham, UK, 10-12 February, pp. 1–6. (2015)
11. Rao, H.: Architecture of Nan'ao multi-terminal VSC-HVDC system and its multi-functional control. CSEE J. Power Energy Syst 1(1), 9–18 (2015)
12. Zheng, Z., Wang, Y., Zhang, D., Song, R., Li, C., Zhang, T.: Reliability evaluation model of zhangbei multi-terminal HVDC transmission system. In: Proc. IEEE International Conference on Energy Internet (ICEI), Nanjing, China, 27-31 May, pp. 279–284. (2019)
13. Hatziargyriou, N., Milanovic, J., Rahmann, C., Ajjarapu, V., Canizares, C., Erlich, I., Hill, D., Hiskens, I., Kamwa, I., Pal, B., Pourbeik, P., Sanchez-Gasca, J., Stankovic, A., Van Cutsem, T., Vittal, V., Vournas, C.: Definition and classification of power system stability: revisited & extended. IEEE Trans. Power Syst. 36(4), 3271–3281 (2021)
14. Kamwa, I., Heniche, A., Trudel, G., Dobrescu, M., Grondin, R., Lefebvre, D.: Assessing the technical value of FACTS-based wide-area damping control loops. In: Proceedings of IEEE/PES General Meeting, pp. 1–10. IEEE, Piscataway (2005)
15. Collados-Rodriguez, C., Cheah-Mane, M., Prieto-Araujo, E.: Gomis-Bellmunt: Stability and operation limits of power systems with high penetration of power electronics. Int. J. Electr. Power Energy Syst. 138(107728), 1–12 (2022)
16. Cheah-Mane, M., Agusti Egea-Alvarez, A., Prieto-Araujo, E., Mehrjerdi, H., Gomis-Bellmunt, O., Xu, L.: Modeling and analysis approaches for small-signal stability assessment of power-electronic-dominated systems. Wiley Interdiscip. Rev.: Energy Environ. 12(1), 1–22 (2023)
17. Tomás-Martín, A., Garcia-Cerrada, A., Sigrist, L., Yagüe, S., Suárez-Porras, J.: State relevance and modal analysis in electrical microgrids with high penetration of electronic generation. Int. J. Electr. Power Energy Syst. 147(108876), 1–13 (2023)
18. Ramasubramanian, D., Vittal, V., Undrill, J.M.: Transient stability analysis of an all converter interfaced generation WECC system. In: Proceedings of Power Systems Computation Conference (PSCC), pp. 1–7. IEEE, Piscataway (2016)
19. Shah, R., Sánchez, J., Preece, R., Barnes, M.: Stability and control of mixed AC-DC systems with VSC-HVDC: a review. IET Gener. Transm. Distrib. 12(10), 2207–2219 (2017)
20. Gu, M., Meegahapola, L., Wong, K.L.: Review of rotor angle stability in hybrid AC/DC power systems. In: Proceedings of IEEE/PES Asia-Pacific Power and Energy Engineering Conference (APPEEC), pp. 1–6. IEEE, Piscataway (2018)
21. Li, Y., Liu, S., Zhu, J., Yuan, X., Xu, Z., Jia, K.: Novel MTDC droop scheme with decoupled power control for enhancing frequency stabilities of weak AC systems. IET Power Generation 14(11), 2007–2016 (2020)
22. Stojković, J., Shetgaonkar, A., Stefanov, P., Lekić, A.: Two-layer control structure for enhancing frequency stability of the MTDC system. Int. J. Electr. Power Energy Syst. 145(108664), 1–12 (2023)
23. Pipelzadeh, Y., Chaudhuri, B., T. C. Green,: Control coordination within a VSC HVDC link for power oscillation damping: A robust decentralized approach using homotopy. IEEE Trans. Control Syst. Technol. 21(4), 1270–1279 (2012)
24. Hadjikypris, M., Terzija, V.: Active power modulation assisting controller scheme implemented on a VSC-HVDC link establishing effective damping of low frequency power oscillations. In: Proceedings of IEEE International Energy Conference (ENERGYCON), pp. 1–6. IEEE, Piscataway (2014)
25. Harnefors, L., Johansson, N., Zhang, L., Berggren, B.: Interarea oscillation damping using active-power modulation of multiterminal HVDC transmissions. IEEE Trans. Power Syst. 29(5), 2529–2539 (2014)
26. Preece, R., Milanovic, J.V.: Tuning of a damping controller for multiterminal VSC-HVDC grids using the probabilistic collocation method. IEEE Trans. Power Delivery 29(1), 318–326 (2014)
27. Eriksson, R.: A new control structure for multi-terminal dc grids to damp inter-area oscillations. IEEE Trans. Power Delivery 31(3), 990–998 (2016)
28. Renedo, J., Garcia-Cerrada, A., Rouco, L., Sigrist, L.: Coordinated design of supplementary controllers in VSC-HVDC multi-terminal systems to damp electromechanical oscillations. IEEE Trans. Power Syst. 36(1), 712–721 (2021)
29. Rodríguez-Cabero, A., Roldán-Pérez, J., Prodanovic, M., Suul, J.A., D'Arco, S.: Virtual friction for oscillation damping and inertia sharing from multi-terminal VSC-HVDC grids. In: Proceedings of IEEE Energy Conversion Congress and Exposition (ECCE), pp. 1–6. IEEE, Piscataway (2020)
30. Xing, Y., Kamal, E., Marinescu, B., Xavier, F.: Advanced control to damp power oscillations with VSC-HVDC links inserted in meshed AC grids. Int. Trans. Electr. Energy Syst. 31(12), 1–22 (2021)
31. Zhao, H., Lin, Z., Wu, Q., Huang, S.: Model predictive control based coordinated control of multi-terminal HVDC for enhanced frequency oscillation damping. Int. J. Electr. Power Energy Syst. 123(106328), 1–12 (2020)
32. Zhang, Z., Zhao, X.: Coordinated power oscillation damping from a VSC-HVDC grid integrated with offshore wind farms: Using capacitors energy. IEEE Trans. Sustainable Energy DOI: 10.1109/TSTE.2022.3224360, 1–11 (2022)
33. Eriksson, R.: Coordinated control of multiterminal dc grid power injections for improved rotor-angle stability based on lyapunov theory. IEEE Trans. Power Delivery 29(4), 1789–1797 (2014)
34. Tang, G., Xu, Z., Dong, H., Xu, Q.: Sliding mode robust control based active-power modulation of multi-terminal HVDC transmissions. IEEE Trans. Power Syst. 31(2), 1614–1623 (2016)
35. Renedo, J., Garcia-Cerrada, A., Rouco, L.: Active power control strategies for transient stability enhancement of AC/DC grids with VSC-HVDC multi-terminal systems. IEEE Trans. Power Syst. 31(6), 4595–4604 (2016)
36. Latorre, H., Ghandhari, M., Söder, L.: Active and reactive power control of a VSC-HVdc. Electr. Power Syst. Res. 78(10), 1756–1763 (2008)
37. Renedo, J., Garcia-Cerrada, A., Rouco, L.: Reactive-power coordination in VSC-HVDC multi-terminal systems for transient stability improvement. IEEE Trans. Power Syst. 32(5), 3758–3767 (2017)
38. Gonzalez-Torres, J.C., Damm, G., Costan, V., Benchaib, A., Lamnabhi-Lagarrigue, L.: A novel distributed supplementary control of Multi-Terminal VSC-HVDC grids for rotor angle stability enhancement of AC/DC systems. IEEE Trans. Power Syst. 36(1), 623–634 (2021)
39. Kundur, P., Klein, M., Rogers, G.J., Zywno, M.S.: Application of power system stabilizers for enhancement of overall system stability. IEEE Trans. Power Syst. 4(2), 614–627 (1989)
40. Renedo, J., Sigrist, L., Garcia-Cerrada, A., Rouco, L.: Modelling of VSC-HVDC multi-terminal systems for small-signal angle stability analysis. In: Proceedings of 15th IET International Conference on AC and DC Power Transmission, pp. 1–7. IET, Stevenage (2019)
41. Cole, S., Beerten, J., Belmans, R.: Generalized dynamic VSC MTDC model for power system stability studies. IEEE Trans. Power Syst. 25(3), 1655–1662 (2010)
42. Cole, S., Belmans, R.: A proposal for standard VSC HVDC dynamic models in power system stability studies. Electr. Power Syst. Res. 81(4), 967–973 (2011)
43. Beerten, J., Cole, S., Belmans, R.: Modeling of multi-terminal VSC HVDC systems with distributed DC voltage control. IEEE Trans. Power Syst. 29(1), 34–42 (2014)

44. Liu, S., Xu, Z., Hua, W., Tang, G., Xue, Y.: Electromechanical transient modeling of modular multilevel converter based multi-terminal HVDC systems. IEEE Trans. Power Syst. 29(1), 72–83 (2014)
45. Saad, H., Peralta, J., Dennetière, S., Mahseredjian, J., Jatskevich, J., Martinez, J.A., Davoudi, A., Saeedifard, M., Sood, V., Wang, X., Cano, J., Mehrizi-Sani, A.: Dynamic averaged and simplified models for MMC-based HVDC transmission systems. IEEE Trans. Power Delivery 28(3), 1723–1730 (2013)
46. Renedo, J., Garcia-Cerrada, A., Rouco, L., Sigrist, L., Egido, I., Sanz Verdugo, S.: Development of a PSS/E tool for power-flow calculation and dynamic simulation of VSC-HVDC multi-terminal systems. In: Proceedings of 13th IET International Conference on AC and DC Power Transmission, pp. 1–6. IET, Stevenage (2017)
47. Beerten, J., Cole, S., Belmans, R.: Generalized steady-state VSC MTDC model for sequential AC/DC power flow algorithms. IEEE Trans. Power Syst. 27(2), 821–829 (2012)
48. Milano, F., Ortega, A.: Frequency divider. IEEE Trans. Power Syst. 32(2), 1493–1501 (2017)
49. Milano, F.: Rotor speed-free estimation of the frequency of the center of inertia. IEEE Trans. Power Syst. 33(1), 1153–1155 (2018)
50. Díez-Maroto, L., Renedo, J., Rouco, L., Fernández-Bernal, F.: Lyapunov stability based wide area control systems for excitation boosters in synchronous generators. IEEE Trans. Power Syst. 34(1), 194–204 (2019)
51. Stubbe (Convener), M.: Long term dynamics phase II. Cigré Task Force 38.02.08 - TB 102, Tech. Rep. (1995).
52. Rouco, L.: Small signal stability toolbox (SSST): Reference manual. Instituto de Investigación Tecnológica (IIT), ETSI ICAI, Universidad Pontificia Comillas, Madrid, Spain, (2002)
53. Pérez-Arriaga, I.J., Verghese, G.C., Schweppe, F.C.: Selective modal analysis with applications to electric power systems, part I: Heuristic introduction. IEEE Trans. Power Appar. Syst. PAS-101(9), 3117–3125 (1982)
54. Verghese, G.C., Pérez-Arriaga, I.J., Schweppe, F.C.: Selective modal analysis with applications to electric power systems, part II: The dynamic stability problem. IEEE Trans. Power Appar. Syst. PAS-101(9), 3126–3134 (1982)
55. Pagola, F.L., Pérez-Arriaga, I.J., Verghese, G.C.: On sensivities, residues and participations: applications to oscillatory stability analysis and control. IEEE Trans. Power Syst. 4(1), 278–285 (1989)
56. Klein, M., Rogers, G.J., Kundur, P.: A fundamental study of inter-area oscillations in power systems. IEEE Trans. Power Syst. 6(3), 914–921 (1991)
57. Chompoobutrgool, Y., Vanfretti, L.: Analysis of time delay effects for wide-area damping control design using dominant path signals. In: Proceedings of IEEE/PES General Meeting, pp. 1–5. IEEE, Piscataway (2014)
58. Zhang, F., Sun, Y., Cheng, L., Li, X., Chow, J.H., Zhao, W.: Measurement and modeling of delays in wide-area closed-loop control systems. IEEE Trans. Power Syst. 30(1), 2426–2433 (2015)
59. Renedo, J., Garcia-Cerrada, A., Rouco, L., Sigrist, L.: Coordinated control in VSC-HVDC multi-terminal systems to improve transient stability: the impact of communication latency. Energies 12, 1–32 (2019)
60. Karlsson, B.: Comparison of PSSE & PowerFactory. Degree Project, Uppsala Universitet, Uppsala, Sweden (2013)
61. Van Cutsem, T., Papangelis, L.: Description, modeling and simulation results of a test system for voltage stability analysis. Tech. Rep., Université de Liège, Belgium (2014)

How to cite this article: Renedo, J., Rouco, L., Garcia-Cerrada, A., Sigrist, L.: Transient stability versus damping of electromechanical oscillations in power systems with embedded multi-terminal VSC-HVDC systems. IET Gener. Transm. Distrib. 17, 3477–3487 (2023). https://doi.org/10.1049/gtd2.12874

APPENDIX A: DATA

A.1 | Data of the test system

Data of the original CIGRE Nordic32A benchmark test system can be found in [51, 60] and a comprehensive description of the system can be found in [61]. Some modifications were made in the test system used in this paper, in order to stress the system and to reduce the damping ratio of inter-area oscillations. The modifications made are detailed in [28]. Converter and HVDC grid parameters are provided in Table A1.

A.2 | Parameters of the control strategies for the case study

- P-WAF: $k_{P,i} = 200$ pu, $\Delta p_{max,i} = 1.0$ pu, $T_{f,i} = 0.1$ s, $T_{W,i} = 10$ s and $\alpha_k = 1/3$. The gains are in nominal p.u. Different values of $k_{P,i}$ are analysed in Section 4.1.
- Q-WAF: $k_{Q,i} = 200$ pu, $\Delta q_{max,i} = 1.0$ pu, $T_{f,i} = 0.1$ s, $T_{W,i} = 10$ s, $V_{TH,i} = 0.75$ pu and $\alpha_k = 1/3$. The gains are in nominal p.u. Different values of $k_{Q,i}$ are analysed in Section 4.1.
- PQ-WAF: The same parameters of strategies P-WAF and Q-WAF are used.

TABLE A1 Converter & HVDC grid data. Base for pu: VSC's nominal apparent power.

Parameters	
Nominal apparent power	1000 MVA
DC voltage	±320 kV
AC voltage	300 kV
Configuration	Symmetrical monopole
Active-power limits	±1000 MW
Reactive-power limits	±450 MVAr
Current limit	1 pu (*d*-axis priority)
DC-voltage limits	±10 %
Max. modulation index ($m_i^{max} = \sqrt{\frac{3}{2}} \cdot \frac{V_{dc,B}}{V_{ac,B}}$)	1.31 pu
Current-controller time constant (τ)	5 ms
Connection impedance: $\bar{z}_s = r_s + jx_s$	0.002 + j0.17 pu
(reactor + 300/400 kV transformer)	
Active-power control	$i_{d,i}^{ref} = p_{s,i}^{ref} / u_{s,i}$
Reactive-power control	$i_{q,i}^{ref} = -q_{s,i}^{ref} / u_{s,i}$
DC-voltage droop parameter ($k_{dc,i}$)	0.1 pu
VSCs' loss parameters (a/b)	11.033 / 3.464 $\times 10^{-3}$ pu
VSCs' loss parameters (c_{rec}/c_{inv})	4.40 / 6.67 $\times 10^{-3}$ pu
DC-line series parameters ($R_{dc,ij}/L_{dc,ij}$)	2.05 Ω / 140.10 mH
DC-line shunt capacitance ($C_{\alpha,ij}$)	1.79 μF
VSC Eq. capacitance ($C_{VSC,i}$)	193.21 μF
Total eq. DC-bus capacitance ($C_{dc,i}$)	195.00 μF